Impulsive Solar X-Ray Bursts. IV. Polarization, Directivity and Spectrum of the Reflected and Total Bremsstrahlung Radiation from a Beam of Electrons Directed Toward the Photosphere

by

Steven H. Langer
Vahé Petrosian

July 1976

SUIPR Report No. 669

National Aeronautics and
Space Administration
Grant NSG 7092 and
Grant NGL 05-020-272

INSTITUTE FOR PLASMA RESEARCH
STANFORD UNIVERSITY, STANFORD, CALIFORNIA

Impulsive Solar X-Ray Bursts. IV. Polarization, Directivity and Spectrum of the Reflected and Total Bremsstrahlung Radiation from a Beam of Electrons Directed Toward the Photosphere

by

Steven H. Langer
Vahé Petrosian

July 1976

SUIPR Report No. 669

National Aeronautics and
Space Administration
Grant NSG 7092 and
Grant NGL 05-020-272

INSTITUTE FOR PLASMA RESEARCH
STANFORD UNIVERSITY, STANFORD, CALIFORNIA

IMPULSIVE SOLAR X-RAY BURSTS. IV. POLARIZATION, DIRECTIVITY AND SPECTRUM OF THE REFLECTED AND TOTAL BREMSSTRAHLUNG RADIATION FROM A BEAM OF ELECTRONS DIRECTED TOWARD THE PHOTOSPHERE

by

Steven H. Langer and Vahé Petrosian

July 1976

SUIPR REPORT NO. 669

National Aeronautics and Space Administration
Grant NSG 7092
and
Grant NGL 05-020-272

Institute for Plasma Research
Stanford University
Stanford, California

IMPULSIVE SOLAR X-RAY BURSTS. IV. POLARIZATION, DIRECTIVITY AND SPECTRUM OF THE REFLECTED AND TOTAL BREMSSTRAHLUNG RADIATION FROM A BEAM OF ELECTRONS DIRECTED TOWARD THE PHOTOSPHERE

Steven H. Langer* and Vahé Petrosian*
Institute for Plasma Research
Stanford University

ABSTRACT

A Monte Carlo method is described for evaluation of the spectrum, directivity and polarization of x-rays diffusely reflected from stellar photospheres. The accuracy of the technique is evaluated through comparison with analytic results. Using the characteristics of the incident x-rays of the model for solar x-ray flares described in the accompanying paper, the spectrum, directivity and polarization of the reflected and the total x-ray fluxes are evaluated. The results are compared with observations.

---

*Also Department of Applied Physics

I. INTRODUCTION

In all models for impulsive solar x-ray bursts the observed x-ray flux is partly due to x-rays emitted directly toward the Earth and partly due to the reflection of x-rays emitted toward the photosphere. In models where the x-rays are produced by a beam of electrons directed toward the photosphere (see Petrosian, 1973, paper I, and the accompanying paper III), the bulk of the x-rays (especially at high energies) are emitted toward the photosphere and the contribution of the reflected x-rays to the observed flux becomes significant.

The general problem of the x-ray albedo of stellar atmospheres and its application x-ray binaries (treated in an approximate analytic manner by Basko, et al, 1974) will be discussed elsewhere. In this paper we present the expected characteristics (spectrum, angular distribution and polarization) of the reflected and total (direct plus reflected) x-ray flux from the model described in the accompanying paper. The Monte Carlo procedure used in the calculation of the reflected x-rays is described in section II. Our results and their comparison with previous results (Tomblin, 1972; Santangelo et al, 1973; Henoux, 1975; Felsteiner and Opher, 1976) are presented in section III. In section IV we summarize the results and comment on their comparison with the observations of the variation of the properties of impulsive x-ray properties with solar longitude.

II. X-ray Albedo of the Solar Photosphere

The problem of diffuse reflection of x-rays from the photosphere is treated by using a Monte Carlo technique where the changes in the

properties of photons (with various initial energies, directions and polarizations) are followed as the photons undergo Compton scattering in the photosphere before they escape or are absorbed by photoionization.

Each photon is characterized by its momentum vector $\vec{k} = k(\sin\theta\cos\varphi, \sin\theta\sin\varphi, \cos\theta)$, its polarization vector $\hat{\epsilon}$ (or the polarization angle ψ between $\hat{\epsilon}$ and the vector $\vec{k} \times \hat{z} \times \vec{k}$) and its depth z in the atmosphere. Instead of z it is more convenient to use the electron column density above z (n = electron density)

$$N(z) = \int_{-\infty}^{z} n(z')\,dz' \qquad (1)$$

At the column density $N \sim 10^{25}\,\mathrm{cm}^{-2}$ where the photons undergo most of their scattering the density scale height is much smaller than the solar radius so the semi-infinite plane parallel atmosphere approximation will be used, and therefore the x and y coordinates of the photon need not enter into the problem (cf., however, the discussion at the end of this section). To further simplify the problem it is assumed that the radiation pattern of the x-ray source has azimuthal symmetry. This amounts to assuming that the magnetic field lines (about which the electrons producing the x-rays spiral, cf. paper III) are radial, this removes any dependence on the azimuthal angle of the direction of observation.

For the energy range (15 to 500 kev) of interest coherent scattering can be neglected (cf. Viegele, Henry and Tracy, 1966) and the scattering electrons (with binding energy $\approx$ thermal energy in the range 10 to 100 ev) can be assumed to be at rest. Thus the Klein-Nishina formula can be

used to describe the scattering process.

$$\frac{d\sigma_{kn}(\theta,\varphi)}{d\Omega} = \frac{3\,\sigma_T}{32\pi}\left(\frac{k'}{k}\right)^2\left[\frac{k'}{k}+\frac{k}{k'}-2+4(\hat{\epsilon}\cdot\hat{\epsilon}')^2\right]$$

$$\frac{k}{k'} = 1+\frac{k}{m_e c^2}\,(1-\cos\theta) \qquad (2)$$

$$\sigma_T = 6.66 \times 10^{-25}\ \mathrm{cm}^{-2}$$

$$(\hat{\epsilon}\cdot\hat{\epsilon}')^2 = \cos^2\theta\,\cos^2\varphi+\sin^2\varphi$$

where $\hat{\epsilon}$, k and $\hat{\epsilon}'$, k' are the photon polarization vector and energy before and after the scattering through relative scattering angles θ and φ. For energies below 70 kev the classical Thomson cross section can be used for $d\sigma$ without loss of accuracy.

The absorption process is described by a photoionization cross section which obeys a k^{-3} power law between K-edges and has discontinuous jumps at the K-edges of the various elements. It is convenient to normalize all cross sections to the total classical Thomson cross section and measure column densities in units of the reciprocal of this number. The photoionization cross section may then be written

$$\sigma_{ph}/\sigma_T = \alpha_i\left(\frac{k}{12.2\ \mathrm{kev}}\right)^{-3},\quad k_i < k < k_{i+1} \qquad (3)$$

The values for α_i are taken from Fireman (1974), with α_i constant between the k-edges at k_i and k_{i+1}. At 12.2 keV $\alpha_i = 1.0$ and the total effective photoionization cross section is equal to the total Compton scattering cross section.

The Monte Carlo Procedure. Consider a photon after the i^{th} scattering at a column density N_i with momentum and polarization vectors $\vec{k}_i$ and $\hat{\epsilon}_i$, characterized by energy k_i and angles θ_i, φ_i and ψ_i relative to the fixed axes described above (for incident photons $i = 0$, $N_0 = 0$).

We first calculate the column density,

$$N_{i+1} = N_i + \delta N \cos\theta_i \ , \qquad (4)$$

where the next event (absorption or scattering) occurs. The column density δN traversed between events is obtained from the solution of

$$R_N = \int_0^{\delta N} e^{-s'\sigma} \, ds' \ , \qquad (5)$$

where R_N is a random number between zero and one. Two column densities δN_{kn} and δN_{ph} are generated using the total Compton scattering and photoionization cross section σ_{kn} and σ_{ph}, respectively. The column density traversed is chosen as $\delta N = \min(\delta N_{kn}, \delta N_{ph})$ and the process associated with the smaller column density occurs unless N_{i+1} turns out to be negative, in which case the photon escapes before the next event. If absorption occurs the position and energy deposited by the photon are recorded.

In the event of scattering the relative scattering angles θ and φ are obtained from

$$R_\theta = \frac{\int_0^\theta d\theta' \sigma_{kn}'(\theta', 2\pi) \cdot \sin\theta'}{\int_0^\pi d\theta' \sigma_{kn}'(\theta', 2\pi) \cdot \sin\theta'} \tag{6}$$

and

$$R_\varphi = \frac{\sigma_{kn}'(\theta, \varphi)}{\sigma_{kn}'(\theta, 2\pi)} \tag{7}$$

where R_θ and R_φ are random numbers between zero and one, and

$$\sigma_{kn}'(\theta, \varphi) \equiv \int_0^\varphi \frac{d\sigma_{kn}(\theta, \varphi')}{d\Omega} \, d\varphi' \quad . \tag{8}$$

These integrals are inverted using a modified regulae falsi numerical method (Conte and DeBoor, 1972). The energy of the scattered photon is

$$k_{i+1} = \frac{k_i}{\left[1 + \left(\frac{k_i}{m_e c^2}\right)\left(1 - \cos\theta\right)\right]} \quad .$$

The polarization angle ψ relative to the coordinate with z-axis parallel to $\vec{k}_i$ (i.e., the angle between $\hat{\epsilon}_{i+1}$ and $\vec{k}_{i+1} \times \vec{k}_i \times \vec{k}_{i+1}$) is determined from an examination of the scattering cross section which can be written as

$$\frac{d\sigma_{kn}}{d\Omega} = \frac{3\sigma_T}{32\pi} \left(\frac{k_{i+1}}{k_i}\right)^2 (\rho_u + \rho_L) \quad , \tag{9}$$

with

$$\rho_u = \frac{k_{i+1}}{k_i} + \frac{k_i}{k_{i+1}} - 2, \quad \rho_L = 4(\hat{\epsilon}_i \cdot \hat{\epsilon}_{i+1})^2 \quad . \tag{10}$$

The ρ_u portion of the cross section corresponds to unpolarized photons and is a relativistic correction. The classical term, ρ_L is a standard dipole scattering contribution. The polarization vector of the scattered photon, $\hat{\epsilon}_{i+1}$, must therefore lie in the plane of the old polarization vector $\hat{\epsilon}_i$ and the new direction of propagation $\vec{k}_{i+1}$. Therefore, if the photon is part of the ρ_L (linearly polarized) component, ψ must satisfy

$$\tan\psi = -\frac{\tan\varphi}{\cos\theta} \quad . \tag{11}$$

Thus, ρ_L should be evaluated at this value of ψ before generating θ and φ;

$$\rho_L = 4(\cos^2\theta \cos^2\varphi + \sin^2\varphi) \quad . \tag{12}$$

The value of ψ is set by generating yet another random number, R_ψ, between zero and one. If $R_\psi > \frac{\rho_u}{\rho_u+\rho_L}$, then ψ is chosen randomly between zero and 2π; otherwise ψ is given by (11).

The values of the angles ψ_i, θ_i, φ_i (relative to the fixed coordinates) after each scattering are kept track of by using a rotation matrix $R(\psi_i, \theta_i, \varphi_i)$ which is the ordinary rotation matrix for Euler angles ψ_i, θ_i, φ_i (see e.g., Mathews and Walker, 1970) and satisfies

$$R^{-1}(\psi,\theta,\varphi) = R_z^{-1}(\varphi)\, R_y^{-1}(\theta)\, R_z^{-1}(\psi)$$

$$R^{-1}(\psi,\theta,\varphi)\hat{k} = \hat{z} \tag{13}$$

$$R^{-1}(\psi,\theta,\varphi)\hat{\epsilon} = \hat{x} \quad .$$

The geometry of the system is shown in figure 1.

When a photon scatters the momentum vector $\hat{k}_{i+1}$ and polarization vector $\hat{\epsilon}_{i+1}$ are given by

$$\begin{aligned} \hat{k}_i &= R^{-1}(\psi,\theta,\varphi)\ \hat{k}_{i+1} \ , \\ \hat{\epsilon}_i &= R^{-1}(\psi,\theta,\varphi)\ \hat{\epsilon}_{i+1} \ . \end{aligned} \tag{14}$$

The Euler angles of the scattered photon relative to the fixed xyz coordinate system, $(\psi_{i+1},\theta_{i+1},\varphi_{i+1})$, are then obtained from

$$R^{-1}(\psi_{i+1},\theta_{i+1},\varphi_{i+1}) = R^{-1}(\psi_i,\theta_i,\varphi_i)\ R^{-1}(\psi,\theta,\varphi) \tag{15}$$

The Generation of the Incident Photons. The incident photons are generated uniformly in the chosen energy band, uniformly in $\cos\theta_0$ within the cone subtended by the photosphere at the x-ray production site, and uniformly in φ_0 in the range 0 to 2π. Each photon is assigned a statistical weight equal to the photon number flux in direction θ_0 at energy k_0 in the incident beam

$$W_0 = J(k_0)\ D(k_0,\theta_0)/k_0 \tag{16}$$

where k_0 is the initial photon energy, J is the integrated flux and D is the directivity (see paper III for the definition of J and D and their form for the model of solar x-ray flares under consideration). This weight is carried with the photon and is used to increment the proper bins in the histograms when the photon escapes.

The initial polarization angle ψ_0 should be generated so as to give, on the average, the degree of polarization $P(k_0,\theta_0)$ of the incident radiation. In general, the incident radiation will be partially linearly polarized and may be decomposed into a combination of unpolarized and linearly polarized light. The linearly polarized and the unpolarized components have relative weight $|P(k_0,\theta_0)|$ and $1 - |P(k_0,\theta_0)|$ respectively. The degree of polarization $P(k_0,\theta_0)$ for the model of impulsive solar x-ray bursts under consideration here is given in paper III. As described there the symmetry of the bremsstrahlung process and the choice of the $\hat{z} - \hat{k}_0$ plane as the $\psi_0 = 0$ reference plane ensures that for $P(k_0,\theta_0) < 0$ the linearly polarized component lies in the direction $\psi_0 = 0$, and for $P(k_0,\theta_0) > 0$ it lies in the direction $\psi_0 = \frac{\pi}{2}$ (normal to the $\hat{z} - \hat{k}_0$ plane). The polarization angle of the incident photon is picked by generating a random number, $R\psi_0$, between 0 and one. If $R\psi_0 < |P(k_0,\theta_0)|$ the photon is linearly polarized (with $\psi_0 = 0$ for $P < 0$ or $\frac{\pi}{2}$ for $P > 0$); otherwise ψ_0 is chosen randomly between 0 and 2π.

As mentioned at the beginning of this section the scattering has been treated in the plane parallel approximation. However, if the source height above the scattering level is comparable to the radius the proper transformation between coordinates referred to the surface normal at the flare site and those referred to the normal at the point of entry into the photosphere should be made, and the inverse transformation should be made for escaping photons.

This process is carried out by rotating the matrix, $R(\psi_0,\tilde{\vartheta}_0,\tilde{\varphi}_0)$, of the photon in flare site coordinates through the angle $\tilde{\theta}$ between the normal at the flare site and the normal at the point

of entry into the photosphere giving the matrix $R(\psi_0,\theta_0,0)$ to be used for the plane parallel approximation as

$$R(\psi_0,\theta_0,0) = R(\psi_0,\tilde{\theta}_0,\tilde{\varphi}_0)\ R^{-1}(0,\bar{\theta},\tilde{\varphi}_0) \tag{17}$$

A photon escaping after the nth scattering, $R(\psi_n,\theta_n,\varphi_n)$, must be referred back to flare coordinates

$$R(\tilde{\psi},\tilde{\theta},\tilde{\varphi}) = R(\psi_n,\theta_n,\varphi_n)\ R(0,\bar{\theta},\tilde{\varphi}_0) \tag{18}$$

The properties of each escaping photon are recorded in the proper histogram bins using the final direction, $\tilde{\theta}$, polarization, $\tilde{\psi}$, and energy, k (the symmetry of the incident flux assures that there is no $\tilde{\varphi}$ dependence).

III. RESULTS

A. Comparison with Previous Work

Before presenting the spectrum, directivity and polarization of the total (reflected plus direct) flux for the model of impulsive solar x-ray bursts described in paper III, we can test the Monte Carlo procedure and evaluate its accuracy through comparisons with earlier work. The problem of scattering from an atmosphere of electrons has been treated previously by several authors using both the classical and relativistic cross sections. Our results can therefore be compared to exact results from the theory of radiation transfer, approximate analytic solutions to the problem of a Compton scattering atmosphere and to previous Monte Carlo solutions.

Chandrasekhar (1960) found the directional and polarization properties of the radiation diffusely reflected by a plane parallel atmosphere of perfect Rayleigh (dipole) scatterers. Abhyankar and Fymat (1971) have extended this calculation to include scatterers with single scattering albedo $\omega_0 = 0.99$.

We have found that with a few thousand photons the Monte Carlo procedure gives results in good agreement with the analytic solutions. An example is shown in figure 2 where we plot the directivity and degree of polarization of the radiation reflected from an azimuthally symmetric (φ_0 chosen randomly between 0 and 2π) incident beam with $\theta_0 = 60^\circ$ and $\psi_0 = 90^\circ$. The directivity is defined as the ratio of the intensity in a given direction to the average intensity and the degree of polarization is the difference between the intensity with polarization perpendicular to and in the meridian plane as a fraction of the total intensity; the meridian plane contains the direction of observation and the normal to the scattering surface. Here we have ignored the Compton shift, i.e., we have set $\sigma_{km} = \sigma_T$, and set $\sigma_{ph} = \sigma_T/99$ to give a single scattering albedo $\omega_0 = 0.99$. The directivity results are good to within the one sigma error bars inferred from the Monte Carlo results, and the degree of polarization results are good to much better than one sigma.

Basko et al (1974), by making various simplifying assumptions, found an analytic approximation for the radiation diffusely reflected by a plane parallel Compton scattering atmosphere. Felsteiner and Opher (1976) have treated the same problem with a Monte Carlo approach. The spectrum of the radiation diffusely reflected in the backward

direction from a beam of unpolarized, normally incident 30 keV photons is shown in figure 3. Our results agree very well with Felsteiner and Opher. Basko et al's approximation III (shown in the figure) locates the single scattering peak and gives about the right height and width (Basko et al used a spread of incident energies between 29 and 30 keV). We find an albedo consistent with Felsteiner and Opher and significantly less than Basko et al which is due to their lower iron abundance.

The problem of the radiation diffusely reflected by a Compton scattering atmosphere from a model spectrum (as opposed to a monochromatic line) has been treated by Tomblin (1972), Santangelo et al (1973), Henoux (1975) and Felsteiner and Opher (1976). Tomblin dealt with energies lower than we treat and Felsteiner and Opher used a thermal bremsstrahlung spectrum which is of interest in the case of x-ray binaries. Santangelo et al treated only the case of an isotropic power law source and did not report results for polarization. In figure 4 we compare our results for the directivity with those of Santangelo et al and Henoux for roughly equivalent isotropic sources. At the lower energy the three curves lie within about 2σ of each other while at the higher energy our results agree very well with those of Henoux and also with Santangelo et al, taking account of the slightly different energy bands.

B. Results for Solar X-ray Bursts

Using the Monte Carlo procedure described in section II we have calculated the spectrum, directivity and polarization of the reflected radiation from the incident beam of the model described in the accompanying paper. Adding the reflected flux to the direct flux we obtain

the spectrum, directivity and polarization of the total flux expected from this model. These predictions for the observable flare properties are presented below.

i) Spectrum

The spectrum of the total flux expected from a power law electron beam (with a differential number flux $\frac{dJ_e}{dE} \propto E^{-\delta-1}$, c.f. paper I, eq. 14) is presented in figure 5. In order to show the detailed properties of the spectrum we have plotted $k^{\delta}\, n(k)$ versus photon energy where $n(k) = J(k)/k$ is the photon number flux (per sec per unit energy interval). As is evident from these curves the steepening of the spectra beyond 100 keV which was present in the direct flux (c.f. papers I and III) becomes more pronounced when the reflected flux is taken into account. Such breaks have been observed (Frost 1969 and Frost and Dennis 1971) during the impulsive (but not the slow) phase of the flare for flares with $\delta \leq 3$. Our model shows that a larger change in the spectral index occurs at 100 keV for harder flares than for softer ones, although experimentally the determination of a break for softer flares would be more difficult.

In Table I we present results from least square fits of the spectra to two power laws, one for photon energies between 20 and 100 keV and another for photon energies greater than 100 keV. The residual variance is much less for the two power law fit than for a single power law fit across the entire energy range. Using the F-test it is possible to test the hypothesis that the data is actually a sample from a single power law with statistical fluctuations and that the reduction in variance with the two power law fit is due simply to the increase in the number of free parameters in the fit. The results show that for none of the

curves can the achieved reduction be expected more than 15% of the time on a statistical basis. Taken as a whole this strongly indicates, but by no means proves, that our model spectra are best fit by a two power law spectrum.

Sometimes such deviations of flare spectra from a single power law are interpreted as indications of a thermal bremsstrahlung of the flare x-rays (c.f., e.g. Elcan 1975). We have therefore fitted our model spectra to a thermal spectrum and determined the temperatures shown in Table I. The thermal spectrum provides a poorer but nevertheless acceptable fit.

We would also like to point out the systematic flattening (or hardening) of the spectrum (in 20 to 100 keV range) of harder flares ($\delta \leq 4$) in going from limb flares ($\cos\theta = 0.0$) to flares at the center of the solar disk ($\cos\theta = -1.0$). Because the majority of flares have δ between 3 and 4, this model indicates that on the average limb flares would be steeper (or softer) than those at the center of the disk although the variation is not as strong as observed (c.f. however, section IV).

TABLE I

Results of Fits to the Spectra

	δ	$\mu \equiv \cos\theta$		
		$0 \leq \mu \leq -0.2$	$-0.4 \leq \mu \leq -0.6$	$-0.8 \leq \mu \leq -1.0$
X^*	3	.55 ± .03	.40 ± .06	.20 ± .08
$20 < k < 100$ keV	4	.57 ± .02	.61 ± .08	.46 ± .09
	5	.61 ± .01	.69 ± .06	.61 ± .11
X^*	3	1.64 ± .04	2.68 ± .26	3.54 ± .96
$k > 100$ keV	4	1.52 ± .03	2.25 ± .07	2.86 ± .54
	5	1.52 ± .01	1.98 ± .07	2.35 ± .16
	3	20.7 ± 3	20.3 ± 3	19.1 ± 3
kT keV	4	16.4 ± 3	15.9 ± 3	15.7 ± 3
	5	13.6 ± 4	13.1 ± 4	12.6 ± 4

$$X^* = \frac{d \log J(k)}{d \log k} + \delta - 1$$

$$J(k) = \text{photon flux in } \frac{\text{keV}}{\text{cm}^2\text{-sec-keV}}$$

Error bars are for a 99% confidence interval.

ii) Directivity

The directivity $\tilde{D}$ of the total outward $(-1 < \cos\theta < 0)$ flux normalized at $\cos\theta = -1$ (center-of-disk flare) is plotted for various energies and index δ in figure 6. (Note that $\tilde{D}(k,\theta) = \frac{J(k,\theta)}{J_T(k, \cos\theta = -1)}$ is defined differently than the directivity D in paper III.) Comparison of these curves with the directivity of the direct flux of paper III show that between 20 and 100 keV the radiation is usually fairly isotropic. For example, at 20 keV the ratio of center to limb flux is 1:6 for the direct flux while for the total flux, in the case of zero pitch angle and an electron energy spectrum with index $\delta = 3$, 4 and 5, these ratios are 1:1, 1:1.5 and 1:1.8, respectively. This structure is even more pronounced at 100 keV, and for $30 < k < 100$ keV and $\delta = 3$ the limb flares $(\cos\theta = 0)$ become weaker than the center-of-disk flares.

Above 100 keV the scattered flux makes a smaller relative contribution due to larger relative energy shifts of the scattered radiation up the steep power law spectrum. The scattered flux also makes a reduced contribution below 20 keV due to stronger absorbtion through photoionization. The result is that outside 20 to 100 keV the directivity is similar to that of the direct flux. The directivity does not depend too strongly on the pitch angle but does tend to decrease with increasing pitch angle.

iii) Polarization

The degree of polarization of the total flux is shown in figure 7. In general, as comparison of these curves with the curves in paper III for the degree of polarization of the direct flux shows, the scattered

flux reduces the degree of polarization from that of the direct flux, but the overall shape is preserved. The degree of polarization decreases both with increasing pitch angle and increasing energy but increases with increasing δ, the power law index. The scattered radiation affects the degree of polarization only slightly because for $\cos\theta \approx -1$, where it dominates, both the direct and scattered flux have zero polarization, while at $\cos\theta \approx 0$, where the direct flux is strongly polarized, there is little scattered flux.

iv) Albedo

The albedo of the solar atmosphere for a monochromatic incident flux is shown in figure 3. In general, for steep spectra of incident flux, such as those occurring in solar x-ray bursts, at a given energy most of the contribution to reflected flux come from incident photons of similar and slightly higher energies with little contribution from much higher energies. Thus, in general, monochromatic albedos will be good approximation for steep power law incident flares. Because of strong directivity of the incident flux of a solar flare, albedo definitions become complicated. On table II we give $D_{REF}(k,\mu)$ the reflect photon number flux as a fraction of the total (integrated overall energies and directions, $\int J(k)dk$) generated flux. For comparison we also show this fraction for the direct flux which is the same as $D(k,\cos\theta)$ [note that $D + D_{REF} \propto \tilde{D}$]. As evident for center-of-disk flares the reflected flux is 5 to 6 times stronger than the direct flux while at the limb the reflected flux contributes only about 35% to the total observed flux.

The observed flux for a given incident electron beam is given by

$$J_{obs}(k,\theta) = \left[D(k,\theta) + D_{REF}(k,\theta) \right] J(k) \quad . \tag{19}$$

Thus with the help of this equation and the relation between $J(k)$ and the incident electron beam one can calculate the total energy of the accelerated electron for observed fluxes at any value of θ.

We also note that most of the photons not reflected are absorbed within three scattering lengths.

TABLE II

Comparison of Direct and Reflected Fluxes at 20 - 25 keV

	δ	$0 < \mu < -0.2$	$-0.8 < \mu < -1.0$
$D_{REF}(k,\mu)$	3	.040	0.122
	4	.052	0.153
	5	.054	0.129
$D(k,\mu)$	3	.078	0.024
	4	.091	0.022
	5	.094	0.021

$\mu = \cos\theta$

$D_{REF}(k,\mu) = J_{REF}(k,\mu) \Big/ J$

$J = \int J(k)dk$ = total incident flux (keV cm^{-2} sec^{-1})

IV. SUMMARY AND CONCLUSIONS

We have developed a Monte Carlo procedure for evaluation of the spectrum, directivity and polarization of x-rays reflected from an atmosphere containing electrons and ions. We have tested the accuracy of this procedure by comparing its results with analytic solutions of similar problems. Our results also agree with previous numerical and Monte Carlo solutions. This program has been used to determine the properties of the reflected x-rays from the solar atmosphere during a solar flare. Using the polarization, spectrum and directivity of the x-rays expected from the model described in paper I and the accompanying paper (paper III), we have calculated the expected properties of the total (reflected plus direct) radiation for various parameters of the model. In comparing the total flux with the direct flux (the flux in absence of reflection) we find the following:

1) The total flux is affected mainly in the 20 to 100 keV range of energies. Above 100 keV the contribution of the reflected radiation is small because of increasing Compton shift with energy, and there is little reflected radiation below 20 keV because of strong photo-absorption at these energies.

2) Because of the above the steepening of the spectrum above 100 keV is more pronounced than that reported on paper I (and is in better agreement with observations by Frost (1969) for the direct flux). We also note that for flares with smaller electron index δ (i.e. harder flares) the spectra tend to be steeper near the solar limb, $\cos\theta = 0$, in comparison with those at the center of the disk, $\cos\theta = -1$. This phenomenon disappears as δ increases. In some cases the curvature produced by this break could result in a spectrum (from a power law electron spectrum) resembling

a thermal bremsstrahlung spectrum indicating that observation of such spectra does not necessarily indicate a thermal origin of the radiation.

3) The directivity of the total flux in the 20 to 100 keV range is reduced considerably in comparison with the directivity of the direct flux. For electron spectra with index $\delta = 3$ the flux is isotropic at 20 - 30 keV, and has the opposite sense of directivity (stronger in the center than at the limb) compared to the direct flux in the 30 - 150 keV range of energies. For higher values of δ directivity is similar to that of the direct flux but the ratios of limb to center fluxes are smaller.

4) In general, the total flux is still highly polarized but the degree of polarization is smaller than that of the direct flux.

In paper II (Petrosian 1974) the properties of the direct flux were compared with the statistical behavior of a sample of flares described by Datlowe, Elcan and Hudson (1974). Two important aspects of this comparison were the absence of variation of frequency of occurrence of flares across the solar disk and steepening of the spectra toward the limb. It was shown that although for the direct flux the spectra are identical across the disk the strong directivity of the direct flux causes favorable conditions for observation of steeper spectra toward the limb. As mentioned above the directivity of the total flux is smaller or non-existent at the 20 - 30 keV range. However, as mentioned in items (2) and (3) above, for values of δ where directivity is small the spectra of the total flux tend to be steeper (or softer) on the limb, while for higher δ where this steepening is absent the flare tend to be stronger toward the limb than at the center.

The situation here is more complicated than that of the direct flux, and the simplified analysis of paper II becomes complicated and not worth being repeated because of its simplicity. However, it can be shown that the above two effects tend to result in gradual steepening of the spectra toward the limb. In fact, an analysis similar to that of paper II shows that for the total flux one can define an equivalent parameter b so that the $b/a\delta'$ term in paper II is about unity implying a difference in spectral index between flares at $-1 < \cos\theta < -\frac{1}{2}$ and at $-\frac{1}{2} < \cos\theta < 0$ of about $+0.5$ instead of the observed 0.7. Note also that because of the smaller value of $b/a\delta'$ the expected frequency of occurrence of flares would be more uniform across the disk (once the H_α visibility factor is taken into account) than for the direct flux.

The negative polarization is in agreement with observations of Tindo et al (1971), but because of the tentative nature of these observations not much more could be inferred from their comparison with the model.

ACKNOWLEDGMENT

We would like to thank the National Center for Atmospheric Research, which is sponsored by the National Science Foundation, for computer time used in this calculation. We would also like to thank Mr. G. Langer of NCAR and Mr. J. Knight for their assistance in the computations. This work was supported by the National Aeronautics and Space Administration under grants NSG 7092 and NGL 05-020-272.

REFERENCES

Abhyankar, K. D. and Fymat, A. L. 1971, Ap. J. Suppl. 23, 35.

Basko, M. M., Sunyaev, R. A. and Titarchuk, L. G. 1974, Astron. & Astrophys. 31, 249.

Chandrasekhar, S. 1960, Radiative Transfer, Dover Publications, Inc., N. Y.

Conte, S. D. and deBoor, C. 1972, Elementary Numerical Analysis, 2nd Ed. McGraw-Hill Book Co.

Datlowe, D. W., Elcan, M. J. and Hudson, H. S., 1974, Solar Phys. 39, 155.

Elcan, M. J. 1975, Bulletin AAS, 7, 422.

Felsteiner, J. and Opher, R. 1976, Astron. & Astrophys., 46, 189.

Fireman, E. L. 1974, Ap. J., 187, 57.

Frost, K. J. 1969, Ap. J., 158, L159.

Frost, K. J. and Dennis, B. R. 1971, Ap. J., 165, 655.

Henoux, J. C. 1975, Solar Phys. 42, 219.

Mathews, J. and Walker, R.L., 1970, Mathematical Methods of Physics, 2nd Ed., W. A. Benjamin, Inc.

Petrosian, V. 1973, Ap. J., 186, 291.

Petrosian, V. 1975, Ap. J., 197, 235.

Santangelo, N., Horstman, H. and Horstman-Moretti, E. 1973, Solar Phys., 29, 143.

Tindo, I. P., Ivanov, V. D., Mandel'stam, S. L. and Shuryghin, A. I. 1972, Solar Phys., 24, 429.

Tomblin, F. F. 1972, Ap. J., 171, 377.

Veigele, W. J., Tracy, P. T. and Henry, E. M. 1966, Am. J. Phys., 34, 1116.

FIGURE CAPTIONS

Figure 1 The Euler angles θ, φ, and ψ which transform the x-axis into the photon polarization vector $\hat{e}$, and the z-axis into the momentum vector $\hat{k}$. Adopted from Mathews and Walker (1970).

Figure 2 Comparison of the Monte Carlo results, represented by circles, with the analytic calculations of Abhyankar and Fymat (1970) (lines), for directivity (open circles and dashed line) and polarization (filled circles and solid line) of scattered radiation from a plane parallel atmosphere consisting of Rayleigh scatterers with single scattering albedo $\omega_0 = 0.99$. The incident beam is normal to the atmosphere ($\cos\theta_0 = 0$, φ_0 uniformly distributed between 0 and 2π) and has polarization vector normal to the meridian plane, $\psi_0 = 0$. Approximately 4,000 emerging photons.

Figure 3 Albedo (normally reflected photon number per keV per sr per incident photon) versus photon energy of an atmosphere containing electrons and ions with "cosmic" abundance ratios for a normal incident monoenergetic beam of 30 keV. The solid line is fitted to the filled circles from this paper. The open circle from Felsteiner and Opher (1976) Monte Carlo results. The dashed line from semi-analytic approximation III of Basko et al (1974) with incident photon energies between 29 and 30 keV and for lower iron abundance.

Figure 4 Comparison of the present Monte Carlo results (solid lines and points with error bars) with those of Henoux (1975) (dashed lines) and Santangelo et al (1973) (dotted lines).

All curves are for an unpolarized incident photon flux of index $\delta = 3$. Lower curves for reflected photon energies $50 < k < 70$ keV; middle curves for $80 < k < 100$ keV; upper curves for $15 < k < 20$ keV except for the dotted line which is for $15 < k < 30$ keV photons. Santangelo et al results are for a lower iron abundance and for $\delta = 2.5$.

Figure 5 Spectrum of total (direct plus reflected) photon flux for various index δ of the incident flux. $n(k)$ = photons per keV per sec; k = photon energy; the curves marked -1 give the flux for $-1 < \cos\theta < -0.8$ (center-of-disk flares) and the curved marked zero give the flux for $-0.2 < \cos\theta < 0$ (limb flares). Pitch angle $\eta = 0$.

Figure 6 Directivity, normalized at $\cos\theta = -1$ (center-of-disk flares), of the total flux for various index δ and energies k in keV. Pitch angle $\eta = 0$ for all curves. For $\eta \neq 0$ directivity is slightly smaller than for $\eta = 0$.

Figure 7 Degree of polarization of the total flux versus $\cos\theta$ for various values of the index δ, pitch angle η and energy k. In (a) all curves are for $\delta = 4$ and are labelled by the value of η in degrees. In (b) curves are labelled by the value of index δ. The dotted line is for an unpolarized incident (or direct) flux and the dashed line gives the polarization of the direct flux at 21.5 keV. Points are from the observations of Tindo et al (1972).

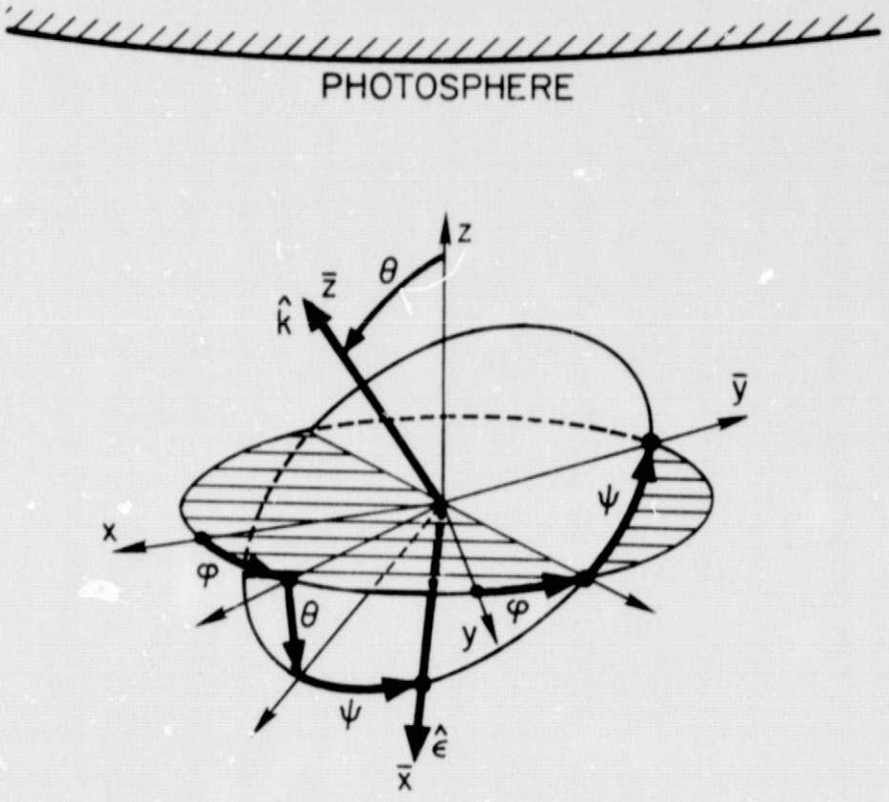

Figure 1

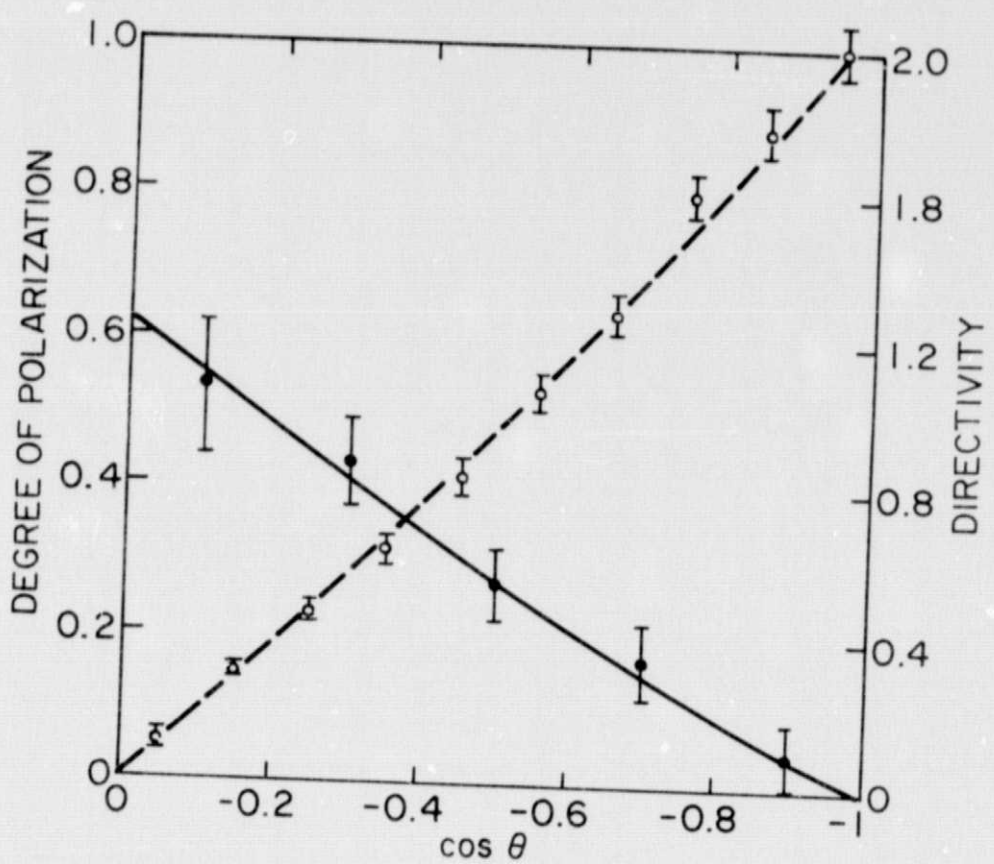
DEGREE OF POLARIZATION
DIRECTIVITY
cos θ
1.0
0.8
0.6
0.4
0.2
0
2.0
1.8
1.2
0.8
0.4
0
-0.2
-0.4
-0.6
-0.8
-1

Figure 2

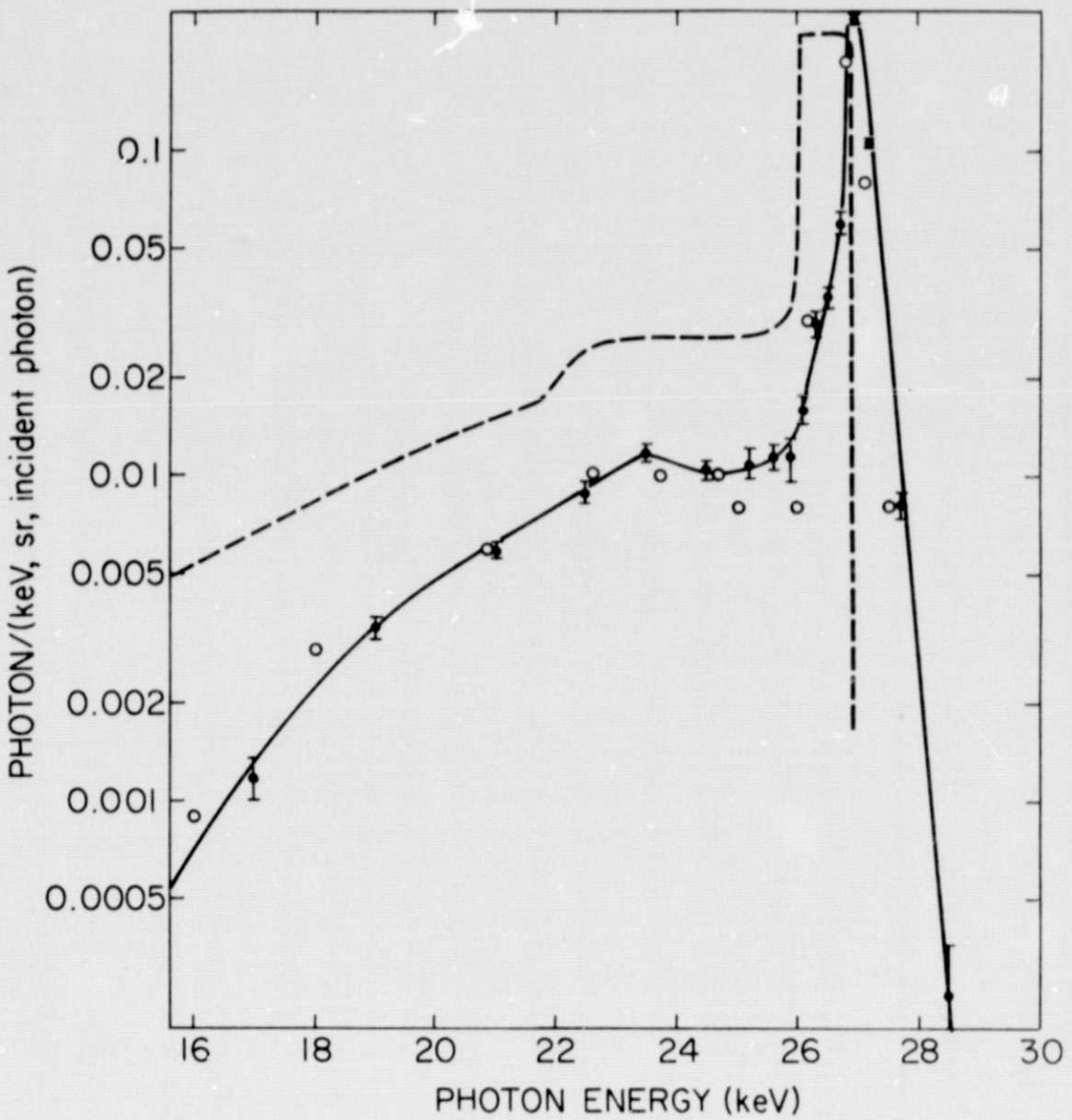
PHOTON/(keV, sr, incident photon)
0.1
0.05
0.02
0.01
0.005
0.002
0.001
0.0005
16
18
20
22
24
26
28
30
PHOTON ENERGY (keV)

Figure 3

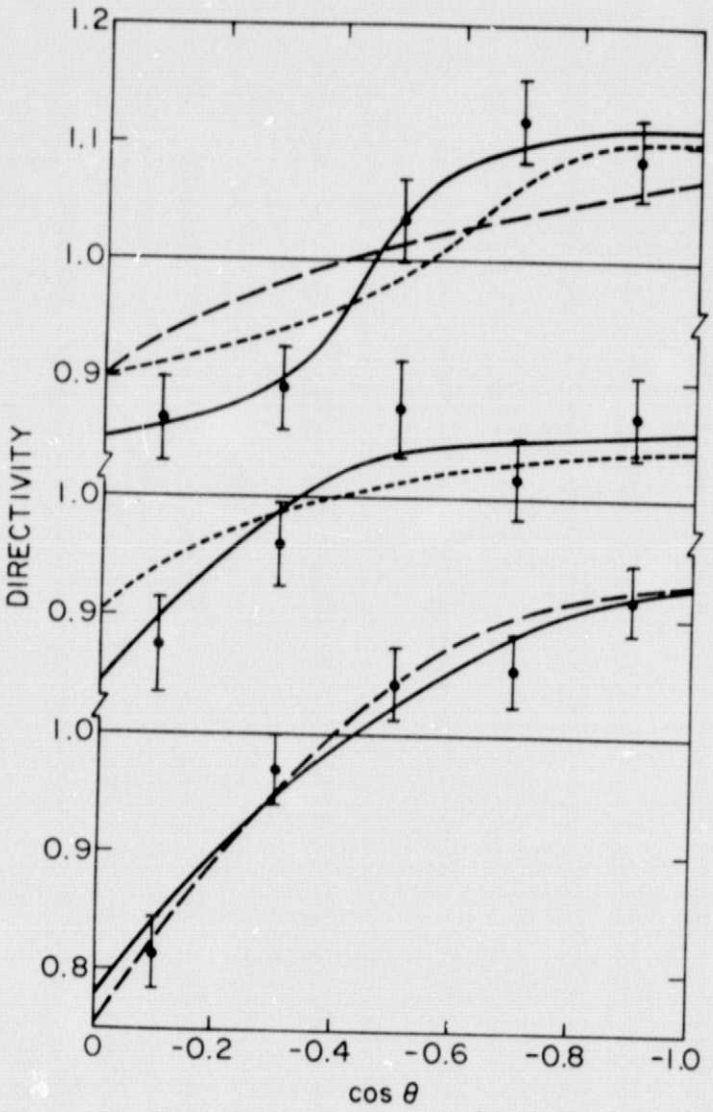

Figure 4

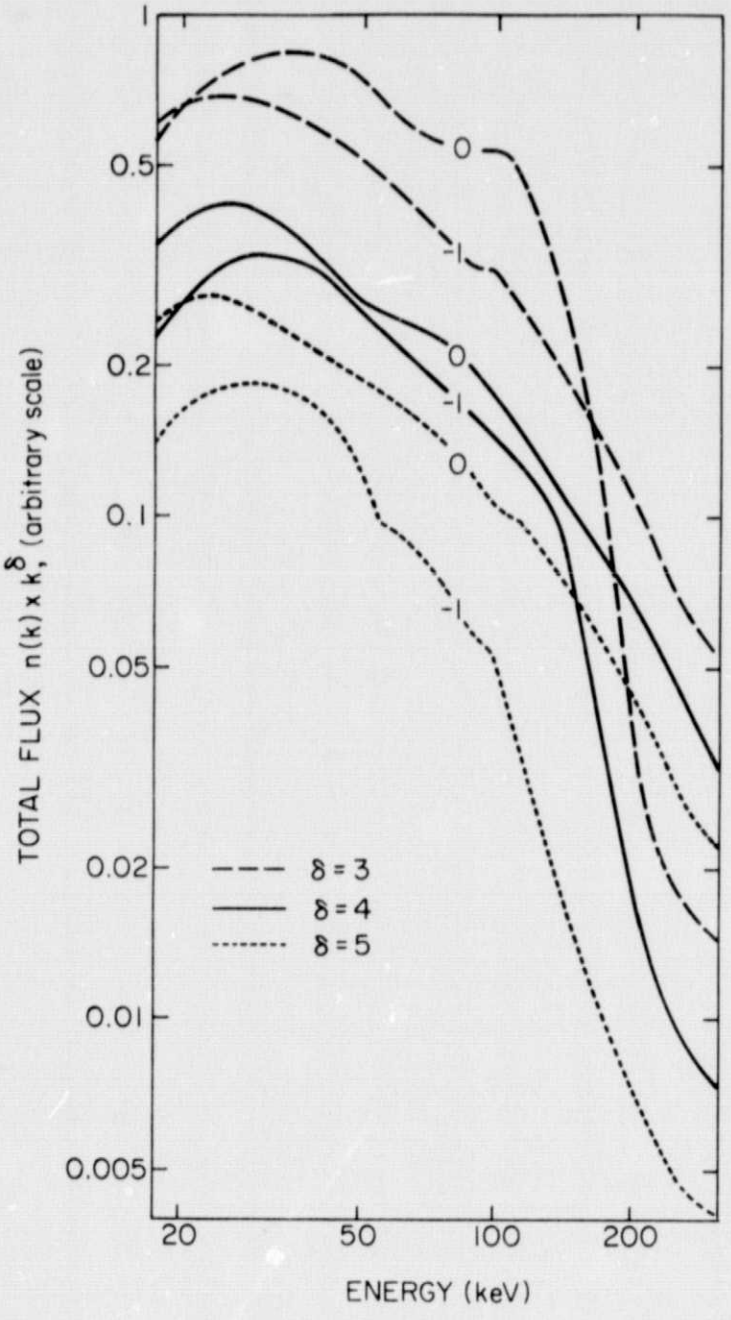
TOTAL FLUX n(k) x k, δ (arbitrary scale)
1
0.5
0.2
0.1
0.05
0.02
0.01
0.005
0
-1
0
-1
0
-1
δ = 3
δ = 4
δ = 5
20
50
100
200
ENERGY (keV)

Figure 5

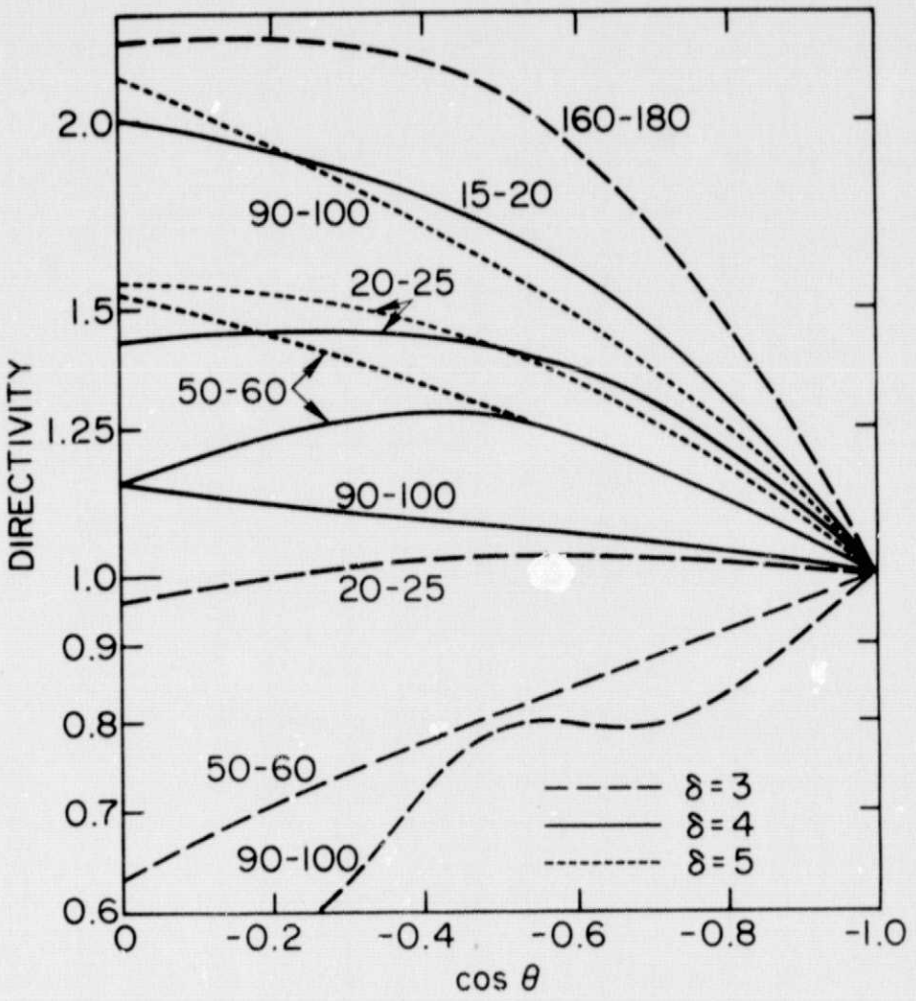
DIRECTIVITY
2.0
1.5
1.25
1.0
0.9
0.8
0.7
0.6
0
-0.2
-0.4
-0.6
-0.8
-1.0
cos θ
160-180
15-20
90-100
20-25
50-60
90-100
20-25
50-60
90-100
δ=3
δ=4
δ=5

Figure 6

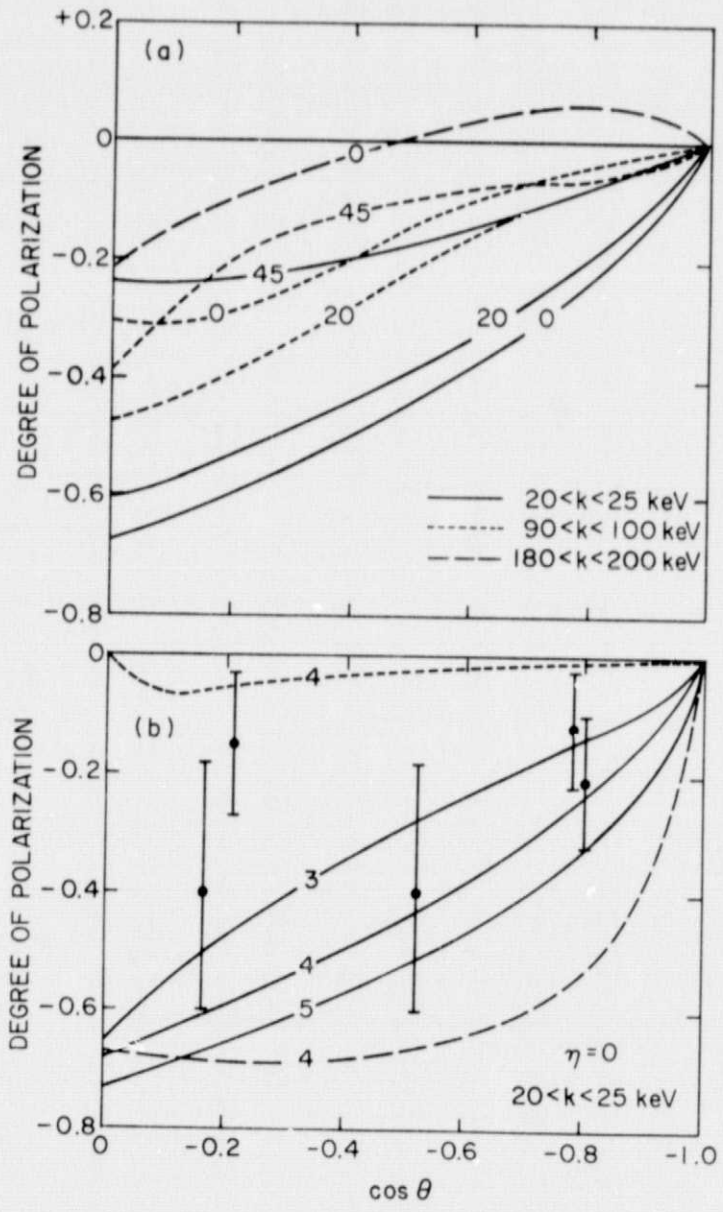
(a)
DEGREE OF POLARIZATION
+0.2
0
-0.2
-0.4
-0.6
-0.8
0
45
45
0
20
20
0
20<k<25 keV
90<k<100 keV
180<k<200 keV
(b)
DEGREE OF POLARIZATION
0
-0.2
-0.4
-0.6
-0.8
4
3
4
5
4
η=0
20<k<25 keV
0
-0.2
-0.4
-0.6
-0.8
-1.0
cos θ

Figure 7